Project 1: Ocean Recharge Oscillator

Student ID: 30832950

Abstract

The El Niño Southern Oscillation (ENSO) is an important mode of ocean-atmosphere variability in the tropical Pacific. ENSO varies between its warm phase (El Niño) and cool phase (La Niña) on timescales of between 2-7 years. This phenomenon oscillates due to the interaction between sea surface temperature (SST) and thermocline depth, driven by surface wind stress. The recharge oscillator model (ROM) is a simple model which approximates the dynamics of ENSO variability. In this model, the cold phase of ENSO is overcome by the 'recharge' of SST anomalies in the eastern Pacific when easterly wind stress drives the convergence of warmer waters in this region. This sets off a positive-feedback loop in which increased ocean SSTs drive convection and further reinforce the recharge. In this study we explore how the choice of time scheme and changes in model physics affect the behaviour of the ROM. To interpret this, we explore the stability of oscillatory behaviour in the model under different conditions, including self-excitation, stochastic forcing and ensemble simulation. We find that, although the ROM exhibits sensitivity to initial conditions, this model is not chaotic when prescribed with random forcing and a time-varying coupling parameter.

The code used for this study can be found in the Github repository: https://github.com/benhutchmet/MTMW14-Assignment-1—ROM

Model Setup

The two ordinary differential equations (ODEs) which describe the behaviour of SST anomalies (T_E) and thermocline depth (h_w) in the recharge oscillator model are as follows (Jin 1997b):

$$\frac{dh_w}{dt} = -rh_w - \alpha bT_e - \alpha\xi_1 \tag{1}$$

$$\frac{dT_E}{dt} = RT_E + \gamma h_w - e_n(h_w + bT_E)^3 + \gamma\xi_1 + \xi_2 \tag{2}$$

Where:

$b = b_0\mu$ represents the thermocline slope determined by the SST-anomaly drive wind stress.

μ is the coupling coefficient.

$b_0 = 2.5$ is a high-end value for the coupling parameter.

$\gamma = 0.75$ is the feedback of the thermocline gradient on the SST gradient.

$c = 1$ represents the damping rate of the SST anomalies.

$R = \gamma b - c$ describes the Bjerknes positive feedback process.

$r = 0.25$ represents the damping of the upper ocean heat content.

$\alpha = 0.125$ relates enhanced easterly wind stress with the recharge of ocean heat content.

e_n varies the degree of non-linearity of the ROM.

ξ_1 represents the random wind stress forcing added to the system.

ξ_2 represents the random heating added to the system.

The results are non-dimensionalised using the following scale factors.

$[T] = 7.5$ K scales the SST anomalies.

$[h] = 150$ m scales the thermocline depth.

$[t] = 2$ months time-scale.

Tasks

Testing the ROM was broken down into 7 tasks from A to G. In each, different conditions for the ROM were considered.

Task A

For Task A, the most simple form of the ROM was considered, with no external forcing ($\xi_{1,2} = 0$) or non-linearity ($e_n = 0$). For this neutral linear case, the ODEs reduce to:

$$\frac{dh_w}{dt} = -rh_w - \alpha bT_e \tag{3}$$

$$\frac{dT_E}{dt} = RT_E + \gamma h_w \tag{4}$$

In this case the model was run with the coupling value set to its critical value ($\mu = \mu_c = 2/3$), which produced stable oscillation with frequency $\omega_c = \sqrt{3/32}$ and period $\tau_c = 2\pi/\omega_c = 41$ months (dimensionalised), as shown in (Jin 1997a).

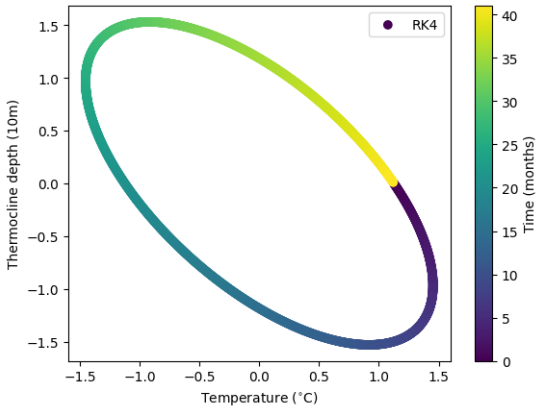

Figure 1: Phase space plot of the solution for the stable neutral ROM in Task A. μ is set to its critical value and there is no external forcing ($\xi_{1,2} = 0$) or non-linearity ($e_n = 0$). Model is run for one period of 41 months with a $\Delta t = 1$ day.

Four time-stepping schemes were used for plotting the time series and phase space of the ROM; explicit euler, modified euler (adams-bashforth), implicit trapezoidal and Runge-Kutta (fourth-order, hence known as RK4).

Figure 1 shows the trajectory of the solution for the RK4 method. Plots for the other time-stepping schemes can be found in the Jupyter notebook (Project_1_30832950.ipynb) in the repository linked. Figure 1 shows stability as the trajectory neither amplifies nor decays with time. Indeed, the only time-stepping scheme which displays apparent instability in Task A is the explicit Euler scheme. The stability of the Euler scheme is analysed by assessing how the amplification matrix A varies with the time step Δt in figure 2.

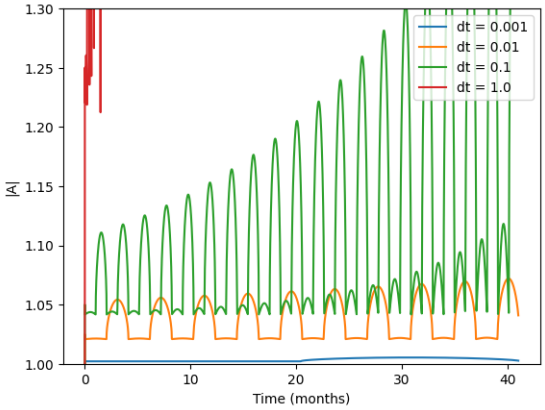

Figure 2: Magnitude of the amplification factor over time for different values of Δt for the Euler time-stepping scheme for the neutral linear ROM (Task A) over 1 time period (41 months).

Figure 2 shows how the explicit Euler scheme is unstable for all Δt tested, as the $|A| > 1$ for each case. The Euler scheme is less unstable for smaller values of $\Delta t \approx 0.001$ and more unstable for larger values of $\Delta t > 0.01$.

Included in the Jupyter notebook is code created by Prof. Pier Luigi Vidale which shows the stability of the RK4 and explicit Euler schemes using plots showing how the amplification factor ($|A|$) varies with $\Re(\lambda)\Delta t$ and $\Im(\lambda)\Delta t$.

Task B

In Task B the stability of the oscillation is explored when sub-critical ($\mu < \mu_c$) and super-critical ($\mu > \mu_c$) values for the coupling parameter are used.

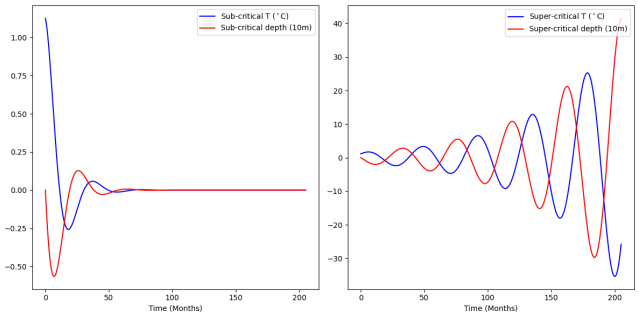

Figure 3: Time series of SST anomalies and thermocline depth for sub-critical ($\mu < \mu_c$) and super-critical ($\mu > \mu_c$) values of the coupling parameter. Run for 5 periods, with $\Delta t = 1$ day, without external forcing ($\xi_{1,2} = 0$) or non-linearity ($e_n = 0$).

Figure 3 shows unstable oscillation for both the sub-critical and super-critical case. In the sub-critical case, the amplitude of the instability decays with time as the coupled system breaks down into two separate modes ($\mu < \mu_c$). In the super-critical case, the system also diverges into two separate modes, but the amplitude of instability increases with time (when $\mu > \mu_c$).

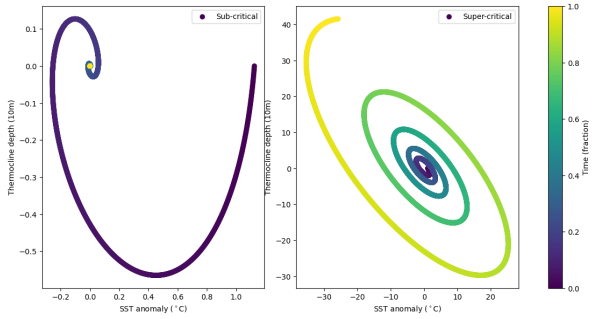

Figure 4: Trajectory of the SST anomalies and thermocline depth for sub-critical ($\mu < \mu_c$) and super-critical ($\mu > \mu_c$) values of the coupling parameter. Run for 5 periods, with $\Delta t = 1$ day, without external forcing ($\xi_{1,2} = 0$) or non-linearity ($e_n = 0$).

In the same way as the time series plots in figure 3, the phase space plots in figure 4 show the decay and amplification of the two different modes with time.

Task C

For the model runs in Task C, the impact of non-linearity is explored by setting $e_n = 0.1$ and resetting the model with

the neutral value for the coupling parameter ($\mu = \mu_c = 2/3$)

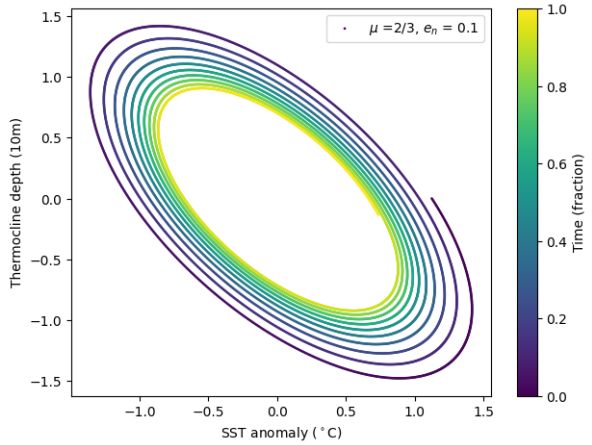

Figure 5: Trajectory of the solution of the nonlinear ROM over 5 periods. μ is set at the critical value where $\mu = \mu_c = 2/3$, there is no external forcing ($\xi_{1,2} = 0$) and $\Delta t = 1$ day.

Similar to the sub-critical case in figure 4, figure 5 appears to decay with time. This is in contrast to figure 1; the linear version of the same plot, which is stable. This decay occurs as the non-linearity term in the SST ODE (2): $-e_n(h_w + bT_E)^3$ becomes the main driver of trajectory due to its scale. The thermocline depth ODE (1) will therefore have much less of an impact on the temperature ODE (2).

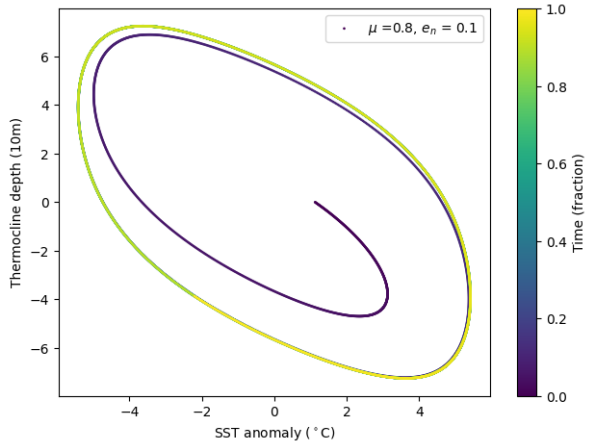

Figure 6: Trajectory of the solution of the nonlinear ROM over 5 periods. μ is set to a super-critical value where $\mu = 0.8$, there is no external forcing ($\xi_{1,2} = 0$) and $\Delta t = 1$ day.

Increasing the value for the coupling coefficient (μ) beyond the critical value in the non-linear case ($e_n = 0.1$) appears to show pseudo-stability in figure 6. As the ROM runs from initial conditions, the non-linearity term drives decay with time, while the super-critical value of μ splits the coupled ROM into two modes which amplify with time. This combination of decay and amplification results in apparent stability with time in figure 6. This suggests that unstable nonlinear cases of the ROM could be tuned by varying μ to achieve some form of stability. Further work could test the stability of this combination of parameters for the ROM.

Task D

The potential for self-excitation of the ROM is explored in Task D. This occurs when ocean recharge events trigger a positive feedback loop between SSTs and atmospheric convection, leading to self-sustained ENSO variability (Munnich, Cane, and Zebiak 1991). In Task D, we allow the coupling parameter to vary on an annual cycle using a relationship from (Galanti and Tziperman 2000).

$$\mu = \mu_0 \left(1 + \mu_{ann} \cos\left(\frac{2\pi t}{\tau} - \frac{5\pi}{6}\right)\right) \quad (5)$$

Where:

$\mu_0 = 0.75$ the standard value for μ.

$\mu_{ann} = 0.2$ the annual range of μ.

τ = 12 months time-scale (which is also non-dimensionalised).

By allowing the coupling parameter to vary on an annual cycle, the ROM can account for how self-excitation processes may be stronger or weaker during different parts of the year. By capturing the potential variability we can test whether the ROM captures observed seasonal variation in ENSO events. Testing this would determine whether the ROM captures self-exciting behaviour.

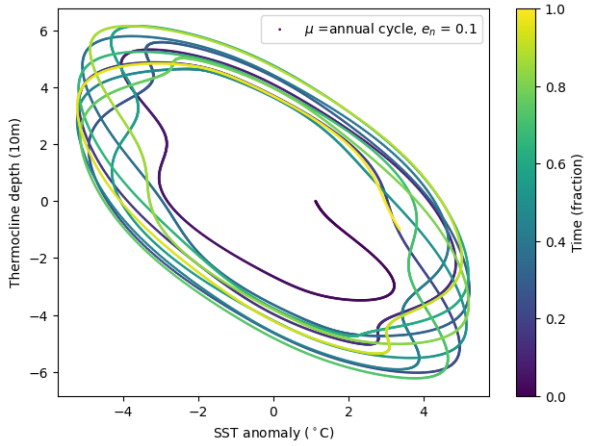

Figure 7: Trajectory of the nonlinear ROM when μ is allowed to vary on an annual cycle according to equation (5). $e_n = 0.1$, $\mu_0 = 0.75$, $\mu_{ann} = 0.2$ and $\tau = 12$ months. The model is run for 5 periods using $\Delta t = 1$ day.

The trajectory of the nonlinear ROM with annual variation in μ appears somewhat stable in figure 7 as the amplitude both decays and amplifies with time. The variability in μ is apparent in the figure as there is a periodic variability to the trajectory. This stable, periodic, variability shows that the ROM captures self-exciting behaviour as the amplitude of the oscillation varies with time.

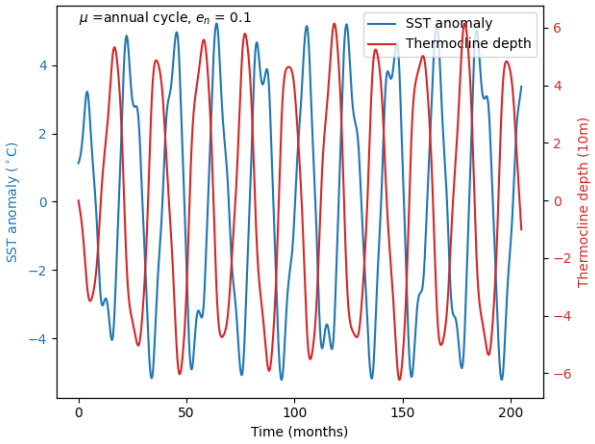

Figure 8: Time series of SST anomalies and thermocline depths for the nonlinear ROM when μ is allowed to vary on an annual cycle according to equation (5). $e_n = 0.1$, $\mu_0 = 0.75$, $\mu_{ann} = 0.2$ and $\tau = 12$ months. The model is run for 5 periods using $\Delta t = 1$ day.

Figure 8 exhibits similar periodic variability to figure 7 whereby ENSO behaviour shows both intrannual (seasonal) and interannual variability. These oscillations are sustained without the need for external forcing, suggesting self-exciting behaviour (Munnich, Cane, and Zebiak 1991).

Task E

For Task D we test the alternative explanation for the variability in ENSO; the stochastic initiation hypothesis. This hypothesis considers the tropical ocean-atmosphere system to be sufficiently unstable such that small fluctuations in external forcings (such as random wind stress) can trigger ENSO events (Thompson and Battisti 2001). This study demonstrated that ENSO variability can be attributed to a combination of external forcing and internal, deterministic dynamics. By running our ROM with both self-exciting and stochastic forcing conditions, we can explore how the balance of these two factors influences ENSO variability. Random wind stress forcing (ξ_1) was added to the ROM model in the following form.

$$\xi_1 = f_{ann} \cos\left(\frac{2\pi t}{\tau}\right) + f_{ran} W \frac{\tau_{cor}}{\Delta t} \qquad (6)$$

Where:

$f_{ann} = 0.02$ annual wind stress forcing.

$f_{ran} = 0.2$ random wind stress forcing.

$\tau_{cor} = 1$ day time-scale (non-dimensionalised)

W is a number between -1 and +1 picked at random, assuming uniform probability.

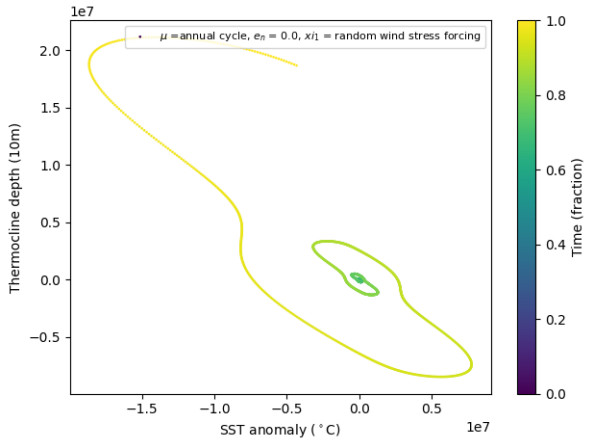

Figure 9: Trajectory of the linear ROM when μ is allowed to vary on an annual cycle according to equation (5) and wind stress forcing ξ_1 is parameterized according to equation (6) . $e_n = 0.0$, $\mu_0 = 0.75$, $\mu_{ann} = 0.2$ and $\tau = 12$ months. The model is run for 5 periods using $\Delta t = 1$ day.

Figure 9 shows rapidly amplifying instability for the linear ROM ($e_n = 0.0$). Initially these instabilities are relatively small, however they soon amplify to scale of 10^7. This occurs as the condition $e_n = 0$ represents a linearization of the nonlinear ROM around a steady state. Stochastic forcing, in the form of random wind stress, causes small fluctuations which perturb the steady state. These perturbations grow over time, eventually leading to the significant instability visible in figures 9 and 10. Additionally, the specification of $\mu_0 = 0.75$, above the critical value ($\mu_c = 2/3$) creates amplifying oscillations that will further perturb the linear scheme (in the same way as the super-critical case in figures 3 and 4).

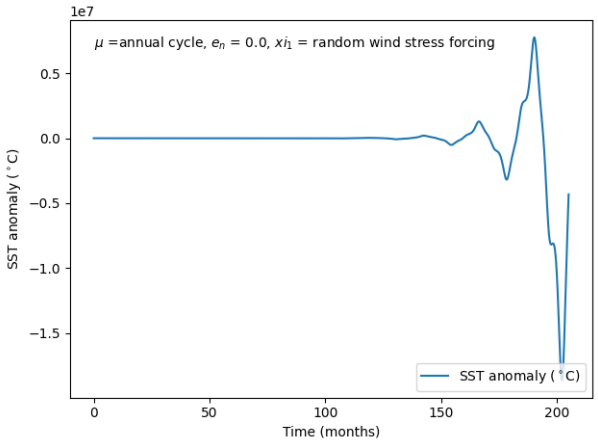

Figure 10: Time series of SST anomalies for the linear ROM when μ is allowed to vary on an annual cycle according to equation (5) and wind stress forcing ξ_1 is parameterized according to equation (6) . $e_n = 0.0$, $\mu_0 = 0.75$, $\mu_{ann} = 0.2$ and $\tau = 12$ months. The model is run for 5 periods using $\Delta t = 1$ day.

The time series in figure 10 shows significant instabilities (order of magnitude 10^7) that amplify with time. This is due

to the random wind stress amplifying as the linear ROM is increasingly perturbed away from its steady state. The linear model therefore captures the underlying nonlinear dynamics of the system.

The significance of stochastic forcing is highlighted in (Flügel and Chang 1996), where the researchers used large ensemble experiments with a linearized ROM to explore the variability of ENSO under different dynamical regimes. The authors found that stochastic forcing had stronger impacts on ENSO variability than nonlinear dynamics at shorter lead times (around 10 months). Beyond this, chaotic dynamics become more important.

Task F

For Task F, a nearly identical model to that used in Task E is considered (with a varying μ, random wind stress ξ_1 and identical parameters), but with non-linearity turned on ($e_n = 0.1$).

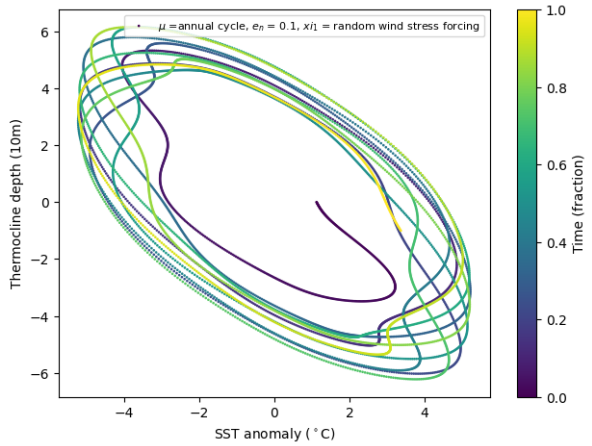

Figure 11: Trajectory of the non-linear ROM when μ is allowed to vary on an annual cycle according to equation (5) and wind stress forcing ξ_1 is parameterized according to equation (6) . $e_n = 0.1$, $\mu_0 = 0.75$, $\mu_{ann} = 0.2$ and $\tau = 12$ months. The model is run for 5 periods using $\Delta t = 1$ day.

Specifying non-linearity ($e_n = 0.1$) in figure 9 returns the ROM to stability (from figure 9). This occurs as the non-linear terms in the ROM act to balance the system and prevent instabilities from growing. Thus, in this iteration of the model the random wind stress forcing (ξ_1) does not propogate into instability as the ROM is returned to stability by the non-linear terms. The random wind stress is visible as a slight 'fuzziness' in figure 11.

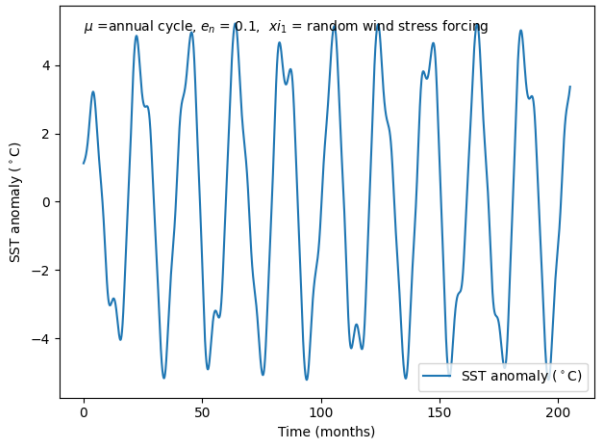

Figure 12: Time series of SST anomalies for the non-linear ROM when μ is allowed to vary on an annual cycle according to equation (5) and wind stress forcing ξ_1 is parameterized according to equation (6) . $e_n = 0.1$, $\mu_0 = 0.75$, $\mu_{ann} = 0.2$ and $\tau = 12$ months. The model is run for 5 periods using $\Delta t = 1$ day.

Figure 10 shows stable oscillations with self-excited variability in a similar way to figure 8. This is due to the non-linear terms balancing out the stochastic forcing in the form of random wind stress.

Task G

To test the behaviour of the ROM under different dynamical regimes we can run the model with perturbations to the initial conditions. In doing this, we can assess whether the model exhibits chaotic behaviour.

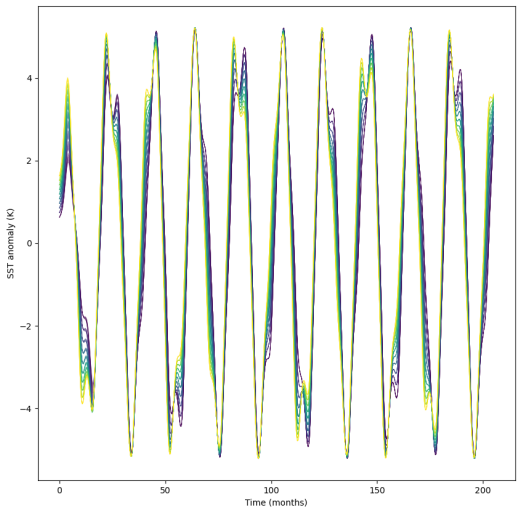

Figure 13: Ensemble time series of SST anomalies for the non-linear ROM when μ is allowed to vary on an annual cycle according to equation (5) and wind stress forcing ξ_1 is parameterized according to equation (6) . $e_n = 0.1$, $\mu_0 = 0.75$, $\mu_{ann} = 0.2$ and $\tau = 12$ months. The ensemble is set up with 10 initial values of T_E between 0.625-1.625 and 10 initial values of h_w between -0.5 and +0.5. The model is run for 5 periods using $\Delta t = 1$ day.

Our model was set up with 10 different initial conditions for both the SST anomalies (T_E) and thermocline depths (h_w). The model was therefore run with 100 different realizations of the initial conditions.

Figure 13 shows variability between the ensemble members in the oscillations of SST anomalies. Generally, there is more spread between the ensemble members at peaks and troughs than between oscillations. This largely reflects the observed SST time series in Figure 1 of (Vallis 1986), where the temperature signal is more variable in each phase of ENSO. This reflects how the ROM is typically more linear between oscillations and exhibits nonlinear states during the peaks and troughs, where differences between ensemble members are amplified. In this way, the ROM appears to show sensitivity to initial conditions (Lorenz 1963), and therefore exhibits chaotic behaviour, in the peaks and troughs of the SST time series. Despite this, the ROM is not necessarily chaotic, as our time series of SST in figure 13 shows more of a periodic signal than the SST observations in figure 1 from (Vallis 1986).

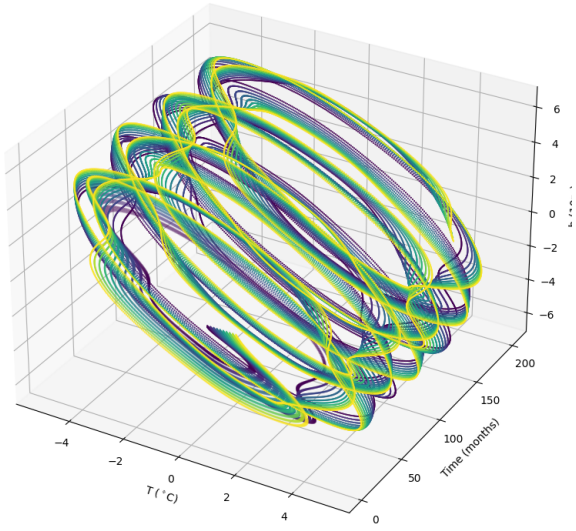

Figure 14: Ensemble trajectories for the non-linear ROM when μ is allowed to vary on an annual cycle according to equation (5) and wind stress forcing ξ_1 is parameterized according to equation (6) . $e_n = 0.1$, $\mu_0 = 0.75$, $\mu_{ann} = 0.2$ and $\tau = 12$ months. The ensemble is set up with 10 initial values of T_E between 0.625-1.625 and 10 initial values of h_w between -0.5-0.5. The model is run for 5 periods using $\Delta t = 1$ day.

Although figure 14 shows sensitivity to initial conditions in the ensemble spread, the ROM is not necessarily chaotic. The attractor in figure 14 shows more periodicity than would typically be expected for a chaotic system. Additionally, there is no indication of bifurcation in the figure, as the ensemble members appear bounded in some way, oscillating in parallel to one another. The attractor in figure 14 does not show the two-lobed, aperiodic structure of the attractor in figure 3b of (Vallis 1986), suggesting less chaotic behaviour in the former system (our ROM). Interestingly (Vallis 1986) notes that systems with two dependent variables (such as our ROM) are limited to stationary or limit-cycle behaviour unless time dependent forcing is added. Our random wind stress forcing is not time-dependent and the ROM does not appear to be chaotic in our ensemble experiment. To induce chaotic behaviour of the ROM, we could increase the strength of the random wind stress forcing or the annual variability of the coupling parameter (μ). Another mechanism for this could involve increasing the non-linearity (by varying e_n) of the system. We could potentially explore how adding a time-dependent forcing for the random heating (ξ_2) term could better replicate observed SST anomalies (Nicholls 1984).

Overall, despite the fact that the ROM does exhibit some chaotic behaviour (sensitivity to initial conditions), the Jin (Jin 1997b) model does not appear chaotic in this study.

References

Flügel, M.; and Chang, P. 1996. Impact of dynamical and stochastic processes on the predictability of ENSO. *Geophysical research letters*, 23(16): 2089–2092.

Galanti, E.; and Tziperman, E. 2000. ENSO's phase locking to the seasonal cycle in the fast-SST, fast-wave, and mixed-mode regimes. *Journal of the atmospheric sciences*, 57(17): 2936–2950.

Jin, F.-F. 1997a. An equatorial ocean recharge paradigm for ENSO. Part I: Conceptual model. *Journal of the atmospheric sciences*, 54(7): 811–829.

Jin, F.-F. 1997b. An equatorial ocean recharge paradigm for ENSO. Part II: A stripped-down coupled model. *Journal of the Atmospheric Sciences*, 54(7): 830–847.

Lorenz, E. N. 1963. Deterministic nonperiodic flow. *Journal of atmospheric sciences*, 20(2): 130–141.

Munnich, M.; Cane, M. A.; and Zebiak, S. E. 1991. A study of self-excited oscillations of the tropical ocean-atmosphere system. *J. Atmos. Sci*, 48: 1238–1248.

Nicholls, N. 1984. The Southern Oscillation and Indonesian Sea Surface Temperature. *Monthly Weather Review*, 112(3): 424 – 432.

Thompson, C.; and Battisti, D. 2001. A linear stochastic dynamical model of ENSO. Part II: Analysis. *Journal of Climate*, 14(4): 445–466.

Vallis, G. K. 1986. El Niño: A chaotic dynamical system? *Science*, 232(4747): 243–245.